Genome-scale analysis of cellular restriction factors that inhibit transgene expression from adeno-associated virus vectors

Ashley M Ngo[1], Andreas S Puschnik[1,2]

[1] Chan Zuckerberg Biohub, San Francisco, CA, USA

[2] Correspondence should be addressed to A.S.P. (andreas.puschnik@czbiohub.org)

ABSTRACT

Adeno-associated virus (AAV) vectors are one of the leading platforms for gene delivery for the treatment of human genetic diseases, but the antiviral cellular mechanisms that interfere with optimal transgene expression are incompletely understood. Here, we performed two genome-scale CRISPR screens to identify cellular factors that restrict transgene expression from recombinant AAV vectors. Our screens revealed several components linked to DNA damage response, chromatin remodeling and transcriptional regulation. Inactivation of the Fanconi Anemia gene FANCA, the Human Silencing Hub (HUSH) associated methyltransferase SETDB1 and the gyrase, Hsp90, histidine kinase and MutL (GHKL)-type ATPase MORC3 led to increased transgene expression. Moreover, SETDB1 and MORC3 knockout improved transgene levels of several AAV serotypes as well as other viral vectors, such as lentivirus and adenovirus. Finally, we demonstrated that inhibition of FANCA, SETDB1 or MORC3 also enhanced transgene expression in human primary cells, suggesting that these could be physiologically relevant pathways that restrict AAV transgene levels in therapeutic settings.

23

24 **IMPORTANCE**

25 Recombinant AAV (rAAV) vectors have been successfully developed for the treatment of
26 genetic diseases. The therapeutic strategy often involves the replacement of a defective gene
27 by expression of a functional copy from the rAAV vector genome. However, cells possess
28 antiviral mechanisms that recognize and silence foreign DNA elements thereby limiting
29 transgene expression and its therapeutic effect. Here, we utilize a functional genomics
30 approach to uncover a comprehensive set of cellular restriction factors that inhibit rAAV-based
31 transgene expression. Genetic inactivation of selected restriction factors increased rAAV
32 transgene expression. Hence, modulation of identified restriction factors has the potential to
33 enhance AAV gene replacement therapies.

34

35 **KEYWORDS**

36 Adeno-associated virus; AAV; viral vector; transgene silencing; HUSH complex; SETDB1; MORC3;
37 Fanconi Anemia; DNA damage; SMC5-SMC6; CRISPR screen; restriction factor; virus-host
38 interaction

39

40 **INTRODUCTION**

41 Adeno-associated virus (AAV) provides a powerful and versatile platform for gene
42 delivery to treat a variety of human genetic diseases. AAV is a small single-stranded DNA virus
43 with a genome size of ~4.7 kb from the *Parvoviridae* family. Its genome consists of two open
44 reading frames, *rep* and *cap*, which are flanked by inverted terminal repeat (ITR) sequences (1,

45 2). The ITRs are the only cis-acting elements required for genome packaging, which enables the
46 generation of recombinant AAV (rAAV) vectors containing a reporter or therapeutic transgene
47 in place of the endogenous *rep* and *cap* genes (3). rAAV vectors have been clinically approved
48 for the treatment of monogenic diseases, such as lipoprotein lipase deficiency, Leber congenital
49 amaurosis and spinal muscular atrophy, and there are over 150 ongoing clinical studies for
50 additional rAAV-based therapies (4).

51 Despite the recent clinical successes, rAAV-based gene therapies face several
52 challenges: (i) Large-scale manufacturing of rAAV for high dose administration (>10^{14} viral
53 particles per patient), is expensive and difficult; (ii) immunological barriers such as the presence
54 of pre-existing neutralizing antibodies against AAV or the triggering of a robust humoral
55 immune response upon treatment prevent (repeated) administration; (iii) hepatic and neuronal
56 genotoxicity has been observed in a number of high-dose administrations; (iv) transgene
57 expression can be lost over time due to the clearance of transduced cells through a cytotoxic T
58 cell response and/or potential silencing of transgene expression (4–6). Increased efficiency in
59 rAAV transgene expression could therefore allow for a reduction in the therapeutic doses
60 needed, which consequently could decrease costs, elicit fewer neutralizing antibodies, reduce
61 the risk of genotoxicity, and lower AAV capsid-directed T lymphocyte-mediated cytotoxicity.
62 However, the precise host cellular pathways that restrict rAAV transgene expression are
63 incompletely understood.

64

65 **RESULTS**

66 **Genome-wide CRISPR screens identify rAAV restriction factors**

67 To identify cellular restriction factors of rAAV transgene expression that are likely to be
68 conserved across multiple cell types, we performed two parallel genome-wide screens using
69 CRISPR knockout (KO) in A549 human lung adenocarcinoma cells and CRISPR interference
70 (CRISPRi) in K562 myelogenous leukemia cells. We used a non-saturating multiplicity of
71 infection (moi) so that inhibition of a repressor would lead to an increase of expression of a
72 fluorescent reporter transgene. Based on rAAV serotype 2 (rAAV2) moi titrations, we used
73 10,000 viral genomes (vg)/cell for the A549 screen and 50,000 vg/cell for the K562 screen
74 (Figure S1A). We performed two rounds of rAAV transduction and FACS-based enrichment of
75 the top 10-20% fluorescent CRISPR library cells followed by analysis of the guide RNA (gRNA)
76 representation via next-generation sequencing (Figure 1A). Analysis with MaGeCK, a
77 computational tool that uses Robust Rank Aggregation (RRA) to identify positively or negatively
78 selected genes, resulted in significant enrichment of 20 genes in the A549 screen and of 88
79 genes in the K562 screens with a cutoff of -log(enrichment score) >5 (Figure S1B and S1C, Table
80 S1 and S2). Nearly all individual gRNAs were enriched for the top 15 genes of both screens,
81 suggesting that the increased transgene expression phenotypes resulting from the genetic
82 perturbations were robust (Figure S1D). Comparison of the enrichment scores from the A549
83 and K562 CRISPR screens highlighted that several Fanconi Anemia (FA) genes, the histone
84 methyltransferase SETDB1, the GHKL-type ATPase MORC3, the SUMO Interacting Motifs
85 Containing 1 (SIMC1), the DNA damage response gene ATM and additional genes (SMCHD1,
86 MTF1, DCLRE1A, DAXX, FAM208A, ZRANB2) were enriched in both datasets (Figure 1B). STRING
87 analysis on the top 100 hits from both screens, identified functional gene clusters and cellular
88 pathways, including the FA pathway, the Human Silencing Hub (HUSH) complex containing the

89 SETDB1 histone methyltransferase, the SMC5-SMC6 complex, the CCR4-NOT complex, and
90 genes linked to DNA damage repair and chromatin regulation (Figure 1C, Table S3).

91 The FA pathway is a biochemical network of 19 genes which are responsible for DNA
92 repair of interstrand crosslinks and stabilization of stalled replication forks, which can impede
93 DNA replication and transcription (7). Most FA core complex components (FANCA-FANCM),
94 which are responsible for lesion recognition and binding, were robustly enriched in both rAAV
95 screens, while the FA factors mediating lesion resolution downstream and the homologous
96 recombination machinery were not or only partially enriched (Figure 1D). Another DNA damage
97 repair factor that scored highly in both screens is the serine/threonine protein kinase ATM
98 (Figure 1B and 1D). ATM activates checkpoint signaling upon double strand breaks, apoptosis
99 and genotoxic stresses, thereby acting as a DNA damage sensor (8). Loss of the FA pathway and
100 ATM is synthetic lethal, suggesting closely linked cellular roles (9). Besides DNA damage
101 response genes, many factors were linked to chromatin and transcriptional regulation (Figure
102 1C and 1D). The histone methyltransferase SETDB1 is recruited by the HUSH complex,
103 composed of FAM208A (also known as TASOR), MPHOSPH8 and PPHLN1, to heterochromatic
104 loci and foreign DNA elements, such as retroviruses and transposons, to mediate transcriptional
105 repression (10, 11). Other HUSH associated factors (MORC2, ZNF638 and ATF7IP) required for
106 recruitment and full epigenetic silencing activity were also enriched in both screens (12–14).
107 The SMC5-SMC6 complex, highly ranked in the K562 screen, was previously shown to play a
108 role in silencing of extrachromosomal HBV DNA as well as unintegrated HIV-1 DNA (Figure 1C
109 and 1D) (15, 16). Finally, MORC3 is a nuclear matrix protein with ATPase activity and has been
110 linked to gene silencing, including of viral pathogens (17–19). Overall, the screens identified

111 numerous candidate restriction factors for rAAV transgene repression, which have canonical
112 roles in DNA damage repair and chromatin regulation.
113
114 **The Fanconi Anemia pathway suppresses transgene expression from rAAV vectors**
115 The FA pathway has to our knowledge not been functionally associated with the
116 regulation of AAV transgene expression. To validate the impact of the FA pathway on rAAV
117 transgene expression, we transduced three sets of FANCA expressing and matched FANCA
118 deficient cells. Dual gRNA/Cas9-mediated deletion of the N-terminus of FANCA in UM-SCC-01
119 cells significantly increased the percentage of rAAV2-tdTomato positive cells (rAAV2+) as well as
120 their median fluorescence intensity (MFI) relative to WT cells (Figure 2A and 2B). This effect was
121 reversed in FANCA transgene-complemented derivatives of the KO cells (Figure 2A and 2B).
122 Furthermore, transduction of mouse ear fibroblasts (MEFs) derived from WT or FANCA KO
123 129S4/SvJaeSor mice showed a similar increase of rAAV transgene expression in the FANCA-
124 deficient background (Figure 2C and 2D). Lastly, we obtained FA patient derived head and neck
125 squamous cell carcinoma cells ("974 cells"), which harbor a FANCA frameshift mutation, as well
126 as corresponding FA patient cells that were lentivirally complemented with an intact FANCA
127 cDNA copy (20). Complementation with FANCA cDNA led to a substantial decrease of rAAV
128 transgene expression relative to the unaltered FA patient derived 974 cells (Figure 2E and 2F).
129 As the FA pathway plays a role in DNA repair, we next tested whether mutations in FANCA
130 affect the stability of rAAV genomes in transduced cells. Quantitative PCR (qPCR) showed that
131 intracellular rAAV genome copy numbers were not significantly different in FANCA KO relative
132 to WT or FANCA trans-complemented UM-SCC1 cells (Figure 2G). Together, these data support

133 that the FA pathway plays a role in the transgene expression from rAAV vectors, independent
134 of rAAV genome stability.
135
136 **Knockout of MORC3 and SETDB1 enhances rAAV transgene expression**
137 Next, we sought to validate the impact of the (GHKL)-type ATPase MORC3 and the
138 histone methyltransferase SETDB1 on rAAV as previous reports have shown antiviral functions
139 for other DNA viruses (10, 14, 18, 19). We generated two clonal A549 KO cells per gene. The
140 MORC3 KO clones harbored frameshift mutations in exon 1, while the SETDB1 KO clones
141 contained a frameshift or large deletion (-21bp) in exon 2 (Figure S2A). The generated KO cell
142 lines did not show any growth defects (Figure S2B). Infection of KO cells with rAAV2-tdTomato
143 showed a substantial increase in rAAV2+ cells (by 16-19% in MORC3 KO and by 22-23% in
144 SETDB1 KO cells 3 days post-infection (dpi)) as well as in MFI (by 2.7-3.3x in MORC3 KO and by
145 5.4-6.8x in SETDB1 KO cells 3dpi) relative to WT cells (Figure 3A, 3B and S3). rAAV transgene
146 expression remained higher in KO vs WT cells over 8 days. Signal decreased in all conditions at
147 later timepoints likely due to the dilution of episomal rAAV DNA during cell proliferation.
148 Lentiviral complementation of MORC3 KO cells with MORC3 cDNA lowered the percentage of
149 rAAV+ cells and MFI to levels observed in WT cells (Figure 3C and 3D), supporting that rAAV
150 transgene expression is indeed modulated by MORC3 activity. Similarly, complementation of
151 SETDB1 KO cells with SETDB1 cDNA decreased both the percentage of tdTomato+ cells (albeit
152 to a lesser degree) and MFI (Figure 3E and 3F). Next, we tested whether deletion of MORC3 or
153 SETDB1 allowed for achieving comparable rAAV transduction rates with reduced rAAV moi.
154 Across a range of 100 to 100,000 vg/cell, MORC3 and SETDB1 KO cells exhibited significantly

155 higher transgene expression levels than WT cells, demonstrating that only ~one-tenth of the
156 rAAV amount was needed in KO cells to achieve similar transgene expression levels as in WT
157 cells (Figure 3G and 3H).

158 To explore whether the restriction factors act on rAAV genome stability or
159 transcriptional regulation, we measured whether rAAV genome copy numbers differed
160 between WT, MORC3 KO and SETDB1 KO cells using qPCR. While the rAAV2 genome copy
161 number was slightly lower in MORC3 KO cells 48h post-transduction, it was increased by 1.7x in
162 SETDB1 KO cells (Figure 3I). Additional quantification of transgene mRNA levels via RT-qPCR
163 showed that expression was moderately increased by 1.1-1.3x in MORC3 KO cells and by >2x in
164 SETDB1 KO cells (Figure S4A). Together, these data indicate that MORC3 likely modulates rAAV
165 transgene expression independently of affecting viral vector genome copies as MORC3 KO
166 exhibited higher tdTomato levels despite lower rAAV genome copies. By contrast, deletion of
167 the histone methyltransferase SETDB1 increased rAAV genome copies, which could largely
168 explain the increase in tdTomato fluorescent levels. However, SETDB1 KO led to an even larger
169 increase in transgene mRNA levels, which means that there could be additional restriction on
170 transcriptional level.

171 Different rAAV serotypes are used in research and clinical applications, often depending
172 on the target cell type or tissue. We therefore assessed whether MORC3 and SETDB1 also
173 affected transgene expression from different rAAV serotypes. We infected cells with rAAV1,
174 rAAV5 and rAAV6 vectors, which only lowly expressed GFP transgene in WT A549 cells. By
175 contrast, GFP expression was drastically increased in MORC3 and SETDB1 KO cells (Figure 4A
176 and 4B). Moreover, rAAV vector genomes can be single-stranded (ssAAV), which require

177 second-strand synthesis prior to gene expression (as were all rAAV vectors used above), or they
178 can be constructed with self-complementary genomes (scAAV). scAAV vectors form intra-
179 molecular dsDNA and thus do not require cell-mediated synthesis of the second strand. We
180 observed that presence of MORC3 and SETDB1 also restricted transgene expression from scAAV
181 genomes, similarly as for ssAAV vectors, which suggests that these cellular restriction factors do
182 not affect processes in the second-strand synthesis (Figure 4C and 4D).
183
184 **Transgene expression from lentiviral, adenoviral and plasmid vectors is inhibited by MORC3**
185 **and SETDB1**
186 In addition to rAAV, other viruses such as lentivirus and adenovirus are used for clinical
187 gene delivery applications (21). Interestingly, several recent studies suggested that MORC3 and
188 SETDB1 can suppress the expression of retroviral elements (10, 19, 22). Consistent with
189 previous studies, both MORC3 and SETDB1 KO increased lentivirus transduction rates and the
190 MFI of encoded GFP across multiple lentiviral dilutions (Figure 5A and 5B). This effect was
191 overall comparable as for rAAV, however, in contrast to rAAV, deletion of MORC3 had a
192 stronger effect on lentiviral transgene expression (e.g. ~12x increase in MFI at 1:3 lentivirus
193 dilution) than deletion of SETDB1 (~8x increase in MFI). RT-qPCR of lentiviral mRNAs showed
194 that transgene expression changes were higher than for rAAV2 in MORC3 KO and SETDB1 KO
195 cells suggesting stronger cellular restriction (Figure S4B). During infection with GFP-expressing
196 adenovirus 5 (AdV5-GFP), the percentage of GFP+ cells and the MFI of GFP were also increased
197 in MORC3 and SETDB1 KO relative to WT cells (Figure 5C and 5D). Moreover, transfection of a
198 GFP-expressing plasmid also led to an increased MFI in MORC3 and SETDB1 KO cells relative to

199 A549 WT cells, although the overall percentage of GFP+ cells did not change (Figure 5E and 5F).
200 By contrast, expression of a fluorescent protein from transfected mRNA-liposomes was
201 unchanged in MORC3 and SETDB1 KO relative to WT cells (Figure 5G and 5H). Together, these
202 data suggest MORC3 and SETDB1 broadly restrict foreign DNA elements, such as viral vectors
203 and plasmid DNA.
204
205 **Knockdown of MORC3 and SETDB1 in primary human fibroblasts leads to increased transgene**
206 **expression**
207 Finally, we explored whether inhibition of MORC3 or SETDB1 activity also affected rAAV
208 transgene expression in untransformed, primary human cells. For this purpose, we performed
209 siRNA knockdown in BJ fibroblasts. Transfection with MORC3 or SETDB1 siRNAs prior to rAAV2-
210 tdTomato transduction increased the percentage of tdTomato+ cells relative to cells
211 transfected with a non-targeting siRNA from 10% to 54% for MORC3 knockdown and to 18% for
212 SETDB1 knockdown (Figure 6A). RT-qPCR confirmed successful knockdown of MORC3 and
213 SETDB1 mRNA levels, although residual expression may still restrict rAAV transgene expression
214 to a certain degree (Figure 6B). Overall, this suggests that the rAAV restriction factors identified
215 in the genome-wide CRISPR screens could have a physiologically relevant function in inhibiting
216 rAAV-based therapies in clinical settings. Additional validation of screen hits beyond FANCA,
217 MORC3 and SETDB1 is needed as well as confirmation in additional primary cells and in vivo
218 models.
219
220 **DISCUSSION**

221 Our study provides a comprehensive picture of the cellular factors that limit gene
222 expression from AAV vectors in human cells. The majority of the identified host genes have
223 known functions in DNA damage sensing and repair, chromatin remodeling and transcriptional
224 regulation. The most prominent hit across both CRISPR screens was the FA pathway, which is
225 critical for the resolution of interstrand crosslinks or stalled replication forks (7). It is plausible
226 that the ITRs in the AAV genome mimic interstrand crosslinks or stalled replication forks and are
227 thus recognized by the FA machinery, which subsequently may impede second-strand synthesis
228 of or transcription from the rAAV genome. Interestingly, another study found that deletion of
229 FANCM led to enhanced AAV template-mediated homologous recombination (23). This further
230 supports that the FA machinery engages with AAV genomes to interfere with both transgene
231 expression as well as AAV template-mediated DNA repair. Other DNA damage response genes
232 enriched in our dataset, e.g. the ATM kinase and the MRN complex (consisting of
233 MRE11A/RAD50/NBN), have been shown to interact with the ITRs in the AAV genome and
234 suppress transgene expression (24–26). Interestingly, studies with other DNA viruses suggested
235 pro-viral effects for the FA pathway, which could be due to distinct differences in their genome
236 structure and life cycle (27–30). Future studies are warranted to mechanistically investigate
237 how the FA pathway interferes with the rAAV vectors and whether FA components directly bind
238 to the AAV genome.

239 Moreover, we found that knockout of the HUSH-associated histone methyltransferase
240 SETDB1 substantially increased transgene expression from rAAV and other viral vectors, such as
241 lentivirus and adenovirus. However, this effect may be partially or largely due to an increase of
242 intracellular rAAV genome copies. The exact mechanism how SETDB1 regulates rAAV genome

243 stability and whether it additionally regulates transcriptional activity from vector genomes need
244 to be studied further. In mammalian cells, SETDB1 is recruited by the HUSH complex to regulate
245 heterochromatin and has been described to mediate silencing of human immunodeficiency
246 virus (HIV) and other retroviral sequences by depositing repressive H3K9me3 histone marks (10,
247 11, 14, 31, 32). Importantly, SETDB1 is able to silence both integrated and unintegrated
248 retroviral DNA (10, 14). rAAV genomes typically exist as unintegrated episomes and are thought
249 to be bound by histones (33). Recently, it was also shown that the HUSH machinery recognizes
250 and silences a broad range of long, intronless transgenes (34). SETDB1 and the HUSH complex
251 may thus be major contributors to rAAV chromatinization and silencing, and potentially tagging
252 heterochromatinized episomes for degradation. The crucial role for SETDB1 and the HUSH
253 complex is further underscored by the enrichment of other factors in our screens. ATF7IP
254 interacts with SETDB1 and protects it from proteasomal degradation (13). The DNA-binding
255 protein ZNF638 (also known as NP220) is responsible for recruitment of the HUSH complex to
256 unintegrated murine retroviral DNA and may also act similarly on rAAV genomes (14). MORC2
257 was shown to to mediate transgene silencing and maintain chromatin compactness upon
258 recruitment by the HUSH complex (12). Finally, the role of the HUSH complex as a rAAV
259 restriction factor was also corroborated by a recent study. Consistent with our data, it showed
260 that knockout of HUSH components resulted in increased rAAV transgene levels and that
261 deletion of ZNF638 (NP220) decreased repressive H3K9me3 histone marks on AAV genomes
262 (35).

263 In addition to the HUSH-associated MORC2, MORC3, another Microchidia CW-type zinc
264 finger protein, was the top hit in the A549 screen and strongly enriched in the K562 screen.

265 MORC proteins are highly conserved, reside in the nucleus, contain a GHKL ATPase domain, and
266 have been linked to heterochromatin condensation and gene silencing (17, 36). Previously,
267 MORC3 was shown to restrict herpesviruses and endogenous retroviruses (ERVs) (18, 19).
268 Mechanistic studies revealed that MORC3 bound to ERV sequences and that knockout of
269 MORC3 resulted in ERV de-repression, reduced H3K9me3 levels and increased chromatin
270 accessibility (19). According to our results, we propose that MORC3 is a critical rAAV restriction
271 factor that silences rAAV genomes through possible chromatin regulation.

272 Additional screen hits have also been linked to chromatin regulation and gene silencing.
273 The ATRX/DAXX complex is responsible for deposition of H3.3 histones at heterochromatic
274 regions and has been shown to associate with both SETDB1 and MORC3 (19, 37, 38). Moreover,
275 the CHAF1 complex, together with the histone chaperon ASF1, delivers newly synthesized
276 H3/H4 dimers to replication forks and was recently shown to mediate silencing of unintegrated
277 HIV-1 DNA (39, 40). Overall, these chromatin modifiers with described roles in foreign DNA
278 silencing and may therefore also be involved in rAAV repression.

279 Lastly, the SMC5-SMC6 complex, which is critical for genome stability and DNA repair
280 (41), has emerged as a component of antiviral responses. It has recently been linked to
281 transcriptional restriction of numerous DNA viruses, such as hepatitis B virus, unintegrated
282 retroviral DNA, papillomavirus and Epstein-Barr virus (15, 16, 42, 43). Our data suggests that
283 SMC5-SMC6 can also potently inhibit rAAV vectors. During DNA repair, this complex is recruited
284 to DNA lesions by FAM178A (also known as SLF2) and SLF1 (44). A recent preprint
285 demonstrated that SIMC1, a top hit in both CRISPR screens and largely with unknown function,
286 forms a distinct complex with FAM178A to localize SMC5/SMC6 to viral replication centers (45).

287 Therefore, it is plausible that rAAV is repressed by recruitment of the SMC5-SMC6 complex via
288 FAM178A/SIMC1.

289 Overall, the identification of multiple components of specific cellular pathways in our
290 CRISPR screens indicates that these are high-confidence candidates for rAAV restriction factors.
291 Of note, two previous siRNA screens for regulators of rAAV transduction in HeLa cells showed
292 enrichment of a subset of the same restriction factors as in our CRISPR screens, including
293 ATF7IP, CHAF1A, DAXX, NPAT (a positive regulator of ATM) and MORC3 (previously named
294 ZCWCC3) in one study, as well as ATF71P, CHAF1A, SETDB1, NPAT and the transcription factor
295 MTF1 in another study (46, 47). Thus, our work corroborates some previously identified
296 candidate restriction factors and expands the network of cellular factors that interfere with
297 rAAV transgene expression.

298

299 **MATERIAL AND METHODS**

300 **Cell Culture**

301 A549 and K562 were obtained from ATCC and cultured in DMEM (Gibco) supplemented with
302 10% fetal bovine serum (Omega Scientific), penicillin/streptomycin (Gibco), non-essential amino
303 acids (Gibco) and L-glutamine (Gibco) at 37C and 5% CO2. HEK293ft cells were obtained from
304 Thermo Scientific and cultured as described above. WT, FANCA KO and trans-complemented
305 FANCA KO UM-SCC1 cells, WT and FANCA KO mouse ear fibroblasts, and FANCA-deficient
306 patient-derived 974 cells with and without FANCA complementation were kindly provided by
307 the Fanconi Anemia Research Fund at Oregon Health & Science University and cultured as
308 described above. Normal human BJ fibroblasts were obtained from ATCC (CRL-2522) and

309 cultured in Knockout DMEM (Gibco) supplemented with 15% fetal bovine serum, 16.5%
310 Medium 199 (Gibco), penicillin/streptomycin, and L-glutamine at 37C and 5% CO2.
311
312 **Viruses**
313 The following rAAV vectors were obtained from the UNC School of Medicine Gene Therapy
314 Center Vector Core: AAV serotype 2 expressing GFP under a chimeric CMV–chicken ß–actin
315 (CBA) promoter (rAAV2-GFP), AAV serotype 2 expressing tdTomato under a CMV immediate
316 enhancer/β-actin (CAG) promoter (rAAV2-tdTomato), AAV serotype 1, 5 or 6 expressing GFP
317 under a CMV promoter (rAAV1/5/6-GFP), and self-complementary AAV serotype 2 expressing
318 GFP under a CMV promoter (scAAV2-GFP). Lentivirus expressing GFP was produced by co-
319 transfection of HEK293ft cells with the following plasmids: plenti-CMV-Puro-DEST (Addgene
320 #17452, gift from Eric Campeau & Paul Kaufman) where GFP cDNA was cloned into the EcoRV
321 site using NEBuilder HiFi DNA Assembly Master Mix; pCMV-dR8.2 dvpr (Addgene, #8455, gift
322 from Bob Weinberg); pCMV-VSV-G (Addgene, #8454, gift from Bob Weinberg); and pAdVAntage
323 (Promega). Supernatants were collected 48h post-transfection, filtered and stored at -80C until
324 use. Adenovirus Serotype 5, Clone Ad5-CMV-hACE2/RSV-eGFP (NR-52390) was kindly provided
325 through BEI Resources.
326
327 **CRISPR screens**
328 A549 cells were stably transduced with lentivirus from lentiCas9-Blast (Addgene #52962, gift
329 from Feng Zhang) and subsequently selected using blasticidin. Next, a total of 240 million A549-
330 Cas9 cells were transduced with the lentivirus of the human GeCKO v2 library (Addgene

331 #1000000049, gift from Feng Zhang) (48) at a moi of 0.4 and selected using puromycin for 7
332 days. 60 million cells of the A549 CRISPR KO library were collected for genomic DNA (gDNA)
333 extraction to assess the reference gRNA distribution. Another 60 million cells were transduced
334 with rAAV2-GFP at a moi of 10,000 vg/cell, which resulted in a ~45-50% transduction rate. The
335 top 10-15% GFP+ cells were sorted 3 dpi and replated. After 7 days, the A549 cells were re-
336 transduced with 10,000 vg/cell and the top 10-15% GFP+ cells were sorted again. A total of ~8
337 million cells was collected for gDNA extraction.
338 K562-dCas9-KRAB cells were a gift from Jonathan Weissman. 240 million cells were transduced
339 with lentivirus from the Human Genome-wide CRISPRi-v2 (Addgene #83969, also gift from
340 Jonathan Weissman) (49) at a moi of 0.4 using spin-inoculation (1000g, 33C, 2h) in 6-well plates.
341 Subsequently, cells were selected using Puromycin for 5 days. 100 million K562 CRISPRi library
342 cells were collected for gDNA extraction to assess the initial gRNA distribution. Another 60
343 million cells were spin-infected (1000g, 33C, 2h) with AAV2-GFP at a moi of 50,000 vg/cell. The
344 top 15-20% GFP+ cells (out of a total %GFP+ of 60%) were sorted and then continued to be
345 cultured. After 7 days, another round of spin-infection with AAV2-tdTomato and FACS of the
346 top 10-15% tdTomato+ cells were performed. A total of 16 million cells were collected for gDNA
347 extraction.
348 For both A549 and K562 cells, gDNA was isolated using the Qiagen DNA Blood Maxi kit (for
349 reference cells) or multiple QIAamp DNA Mini kit columns (for sorted cells). CRISPR gRNA
350 encoding DNA sequences were amplified in a two-step nested PCR using KAPA HiFi HotStart
351 ReadyMixPCR Kit (Kapa Biosystems). In the first PCR step, 36-48 reactions and 12 reactions
352 containing 6 µg gDNA were set up for the reference and sorted samples, respectively, and

353 amplified for 16 cycles. Reactions for each sample were pooled and mixed. In the second PCR
354 step, 4 reactions containing 5 µl PCR1 product were amplified for 12 cycles using indexed
355 primers. PCR products were gel purified using QIAquick Gel Extraction Kit and sequenced on an
356 Illumina NextSeq 500 using custom sequencing primers. Primers sequences are listed in Table
357 S4.
358 For analysis, demultiplexed FASTQ files were aligned to gRNA reference table and enrichment
359 of each gRNA was calculated by comparing the relative abundance in the selected and
360 unselected cell population. Gene enrichment analysis was performed using MaGeCK (50). For
361 STRING analysis (51), the top 100 enriched genes from each CRISPR screen were used as input
362 and gene interactions were computed using a STRING confidence score of 0.4. MaGeCK scores
363 were overlaid using Cytoscape 3.9.0 (52) and only the major gene network is displayed in Figure
364 1.
365
366 **Generation of KO cell lines**
367 DNA oligos (Integrated DNA Technologies) containing gRNA sequences complementary to
368 MORC3 or SETDB1 genomic loci were annealed and ligated into pX458 (Addgene #48138, gift
369 from Feng Zhang). A549 cells were transfected with pX458 constructs using Lipofectamine 3000
370 and two days later GFP-positive cells were single-cell sorted into 96-well plates containing
371 complete media. After several weeks, gDNA was isolated from obtained cell clones using
372 QuickExtract (Lucigen), the gRNA-targeted sites were PCR-amplified, PCR products Sanger-
373 sequenced and sequences aligned to reference sequences using Geneious Prime. A list of all
374 used gRNA oligo and genotyping primer sequences can be found in Table S4.

375

376 **Lentiviral complementation of KO cells**

377 For generation of trans-complemented cell lines, lentivirus was generated as described above
378 using plenti-CMV-Puro-DEST containing MORC3 (OriGene Technologies, RC210530) or SETDB1
379 (OriGene Technologies, RC226620) cDNA sequences. KO cells were transduced in presence of
380 polybrene and subsequently selected using Puromycin.

381

382 **Flow cytometry**

383 Cells were plated in 96-wells and infected the next day. At indicated timepoints, cells were
384 trypsinized and analyzed by flow cytometry using a Cytoflex S flow cytometer (Beckman
385 Coulter). At least 4,000 cells were recorded per sample and cells were gated based on FSC/SSC,
386 FSC-H/FSC-A (singlets) and finally PE (tdTomato) or FITC (GFP) to determine the percentage of
387 fluorescent (infected) cells using FlowJo 10. Moreover, the median fluorescence intensity (MFI)
388 of the fluorescent cells was determined using FlowJo 10. In all experiments, uninfected cells
389 served as negative control for gate setting.

390

391 **Quantification of intracellular AAV genome copies**

392 UM-SCC1 or A549 cell lines were plated in 12-well plates and transduced with rAAV2-tdTomato
393 at a moi of 10,000 vg/cell the next day. 48h post-transduction cells were washed with PBS 3
394 times, trypsinized and pelleted by centrifugation. Cellular and rAAV DNA was extracted from
395 cell pellet using the DNeasy Blood and Tissue kit (Qiagen). 2 µl of purified DNA was used as
396 input to quantify AAV genome copies via qPCR on a Bio-Rad CFX96 Touch system. AAV genomes

397 copies were determined by amplification with primers targeting the AAV2 ITR region and
398 normalized to the cellular RPPH1 locus copy number using IDT PrimeTime qPCR primers. QPCR
399 primer sequences can be found in Table S4.
400
401 **RT-qPCR**
402 For quantification of transgene expression, AAV- or lentivirus transduced cells were harvested
403 using the Power SYBR Green Cells-to-CT kit (Invitrogen). After reverse transcription,
404 quantitative PCR was performed on a Bio-Rad CFX96 Touch system and viral transgene levels
405 (GFP or tdTomato) were normalized to cellular 18S levels. For quantification of siRNA
406 knockdown of MORC3 and SETDB1 mRNA levels, cells were harvested 4 days post siRNA
407 transfection using the Power SYBR Green Cells-to-CT kit (Invitrogen). IDT PrimeTime qPCR
408 Primers for MORC3 and SETDB1 were used and expression levels were normalized to 18S. QPCR
409 primer sequences can be found in Table S4.
410
411 **Cell proliferation assay**
412 WT, MORC3 KO and SETDB1 KO cells were seeded in 96-wells at a density of 8,000 cells per
413 well. At 24, 48 and 72h post-plating Cell Titer Glo 2.0 solution (Promega) was added on top of
414 the cell media and incubated for 10min. After that, 100 µl were transferred to a white 96-well
415 microplate and luminescence was measured using on an EnVision plate reader (PerkinElmer).
416
417 **siRNA transfection**

418 ON-TARGETplus Non-targeting Control Pool, ON-TARGETplus Human MORC3 siRNA SMART
419 POOL and ON-TARGETplus Human SETDB1 siRNA SMART POOL were obtained from Horizon
420 Discovery.
421 10,000 BJ fibroblasts were plated in 96-wells to reach ~50% confluency by the next day. Then,
422 cells were transfected with siRNA pools using 0.3 µl RNAiMAX reagent (Invitrogen), 30 nM
423 siRNA and 20 µl OptiMEM (Gibco) per 96-well. 4 days post-transfection, cells were transduced
424 with rAAV and rAAV transgene expression was quantified by flow cytometry 36h post-
425 transduction. In parallel, transfected but untransduced cells were harvested for analysis of
426 mRNA knockdown.
427
428 **DATA AVAILABILITY**
429 The raw sequencing data for the A549 CRISPR KO and K562 CRISPRi screens are available on
430 NCBI under the BioProject ID PRJNA852611.
431
432 **ACKNOWLEDGMENTS**
433 We thank Drs. Nicole Paulk (UCSF), Jan Carette (Stanford University) and James Zengel
434 (Stanford University) for helpful discussions; the Biohub Genomics Platform for help with
435 sequencing of the CRISPR screen samples; the UNC Gene Therapy Center for providing rAAV
436 vectors; Drs. Jonathan Weissman (UCSF) and Feng Zhang (Broad Institute) for providing the
437 CRISPRi and CRISPR KO library plasmids; and Dr. Leslie Wakefield and the Fanconi Anemia
438 Research Fund at Oregon Health & Science University for providing FANCA KO and trans-
439 complemented cell lines.

440

441 **AUTHOR CONTRIBUTIONS**

442 AMN and ASP performed all experiments and analyzed data. ASP designed the study and wrote

443 the manuscript.

444

445 **DECLARATION OF INTERESTS**

446 The authors have declared no competing interest.

447

448 **REFERENCES**

449 1. Srivastava A, Lusby EW, Berns KI. 1983. Nucleotide sequence and organization of the adeno-

450 associated virus 2 genome. J Virol 45:555–564.

451 2. Samulski RJ, Muzyczka N. 2014. AAV-Mediated Gene Therapy for Research and Therapeutic

452 Purposes. Annu Rev Virol 1:427–451.

453 3. McLaughlin SK, Collis P, Hermonat PL, Muzyczka N. 1988. Adeno-associated virus general

454 transduction vectors: analysis of proviral structures. J Virol 62:1963–1973.

455 4. Wang D, Tai PWL, Gao G. 2019. Adeno-associated virus vector as a platform for gene therapy

456 delivery. 5. Nat Rev Drug Discov 18:358–378.

457 5. Colella P, Ronzitti G, Mingozzi F. 2018. Emerging Issues in AAV-Mediated In Vivo Gene

458 Therapy. Molecular Therapy - Methods & Clinical Development 8:87–104.

459 6. Greig JA, Breton C, Martins KM, Zhu Y, He Z, White J, Bell P, Wang L, Wilson JM. 2022. Loss of
460 transgene expression limits liver gene therapy in primates. bioRxiv
461 https://doi.org/10.1101/2022.03.24.485675.

462 7. Ceccaldi R, Sarangi P, D'Andrea AD. 2016. The Fanconi anaemia pathway: new players and
463 new functions. 6. Nat Rev Mol Cell Biol 17:337–349.

464 8. Maréchal A, Zou L. 2013. DNA Damage Sensing by the ATM and ATR Kinases. Cold Spring
465 Harb Perspect Biol 5:a012716.

466 9. Cai M-Y, Dunn CE, Chen W, Kochupurakkal BS, Nguyen H, Moreau LA, Shapiro GI, Parmar K,
467 Kozono D, D'Andrea AD. 2020. Cooperation of the ATM and Fanconi Anemia/BRCA
468 Pathways in Double-Strand Break End Resection. Cell Reports 30:2402-2415.e5.

469 10. Tchasovnikarova IA, Timms RT, Matheson NJ, Wals K, Antrobus R, Göttgens B, Dougan G,
470 Dawson MA, Lehner PJ. 2015. Epigenetic silencing by the HUSH complex mediates
471 position-effect variegation in human cells. Science 348:1481–1485.

472 11. Liu N, Lee CH, Swigut T, Grow E, Gu B, Bassik MC, Wysocka J. 2018. Selective silencing of
473 euchromatic L1s revealed by genome-wide screens for L1 regulators. Nature 553:228–232.

474 12. Tchasovnikarova IA, Timms RT, Douse CH, Roberts RC, Dougan G, Kingston RE, Modis Y,
475 Lehner PJ. 2017. Hyperactivation of HUSH complex function by Charcot-Marie-Tooth
476 disease mutation in MORC2. Nat Genet 49:1035–1044.

477 13. Timms RT, Tchasovnikarova IA, Antrobus R, Dougan G, Lehner PJ. 2016. ATF7IP-Mediated
478 Stabilization of the Histone Methyltransferase SETDB1 Is Essential for Heterochromatin
479 Formation by the HUSH Complex. Cell Rep 17:653–659.

480 14. Zhu Y, Wang GZ, Cingöz O, Goff SP. 2018. NP220 mediates silencing of unintegrated
481 retroviral DNA. 7735. Nature 564:278–282.

482 15. Decorsière A, Mueller H, van Breugel PC, Abdul F, Gerossier L, Beran RK, Livingston CM,
483 Niu C, Fletcher SP, Hantz O, Strubin M. 2016. Hepatitis B virus X protein identifies the
484 Smc5/6 complex as a host restriction factor. 7594. Nature 531:386–389.

485 16. Dupont L, Bloor S, Williamson JC, Cuesta SM, Shah R, Teixeira-Silva A, Naamati A,
486 Greenwood EJD, Sarafianos SG, Matheson NJ, Lehner PJ. 2021. The SMC5/6 complex
487 compacts and silences unintegrated HIV-1 DNA and is antagonized by Vpr. Cell Host
488 Microbe 29:792-805.e6.

489 17. Moissiard G, Cokus SJ, Cary J, Feng S, Billi AC, Stroud H, Husmann D, Zhan Y, Lajoie BR,
490 McCord RP, Hale CJ, Feng W, Michaels SD, Frand AR, Pellegrini M, Dekker J, Kim JK,
491 Jacobsen SE. 2012. MORC family ATPases required for heterochromatin condensation and
492 gene silencing. Science 336:1448–1451.

493 18. Sloan E, Orr A, Everett RD. 2016. MORC3, a Component of PML Nuclear Bodies, Has a Role
494 in Restricting Herpes Simplex Virus 1 and Human Cytomegalovirus. Journal of Virology
495 90:8621–8633.

496 19. Groh S, Milton AV, Marinelli LK, Sickinger CV, Russo A, Bollig H, de Almeida GP, Schmidt A,
497 Forné I, Imhof A, Schotta G. 2021. Morc3 silences endogenous retroviruses by enabling
498 Daxx-mediated histone H3.3 incorporation. Nat Commun 12:5996.

499 20. Webster ALH, Sanders MA, Patel K, Dietrich R, Noonan RJ, Lach FP, White RR, Goldfarb A,
500 Hadi K, Edwards MM, Donovan FX, Jung M, Sridhar S, Fedrigo O, Tian H, Rosiene J,
501 Heineman T, Kennedy JA, Bean L, Rosti O, Tryon R, Gonzalez A-M, Rosenberg A, Luo J-D,
502 Carrol T, Velleuer E, Rastatter JC, Wells SI, Surrallés J, Bagby G, MacMillan ML, Wagner JE,
503 Cancio M, Boulad F, Scognamiglio T, Vaughan R, Koren A, Imielinski M, Chandrasekharappa
504 S, Auerbach AD, Singh B, Kutler DI, Campbell PJ, Smogorzewska A. 2021. Fanconi Anemia
505 Pathway Deficiency Drives Copy Number Variation in Squamous Cell Carcinomas. bioRxiv
506 https://doi.org/10.1101/2021.08.14.456365.

507 21. Bulcha JT, Wang Y, Ma H, Tai PWL, Gao G. 2021. Viral vector platforms within the gene
508 therapy landscape. Sig Transduct Target Ther 6:1–24.

509 22. Collins PL, Kyle KE, Egawa T, Shinkai Y, Oltz EM. 2015. The histone methyltransferase
510 SETDB1 represses endogenous and exogenous retroviruses in B lymphocytes. Proceedings
511 of the National Academy of Sciences 112:8367–8372.

512 23. de Alencastro G, Puzzo F, Pavel-Dinu M, Zhang F, Pillay S, Majzoub K, Tiffany M, Jang H,
513 Sheikali A, Cromer MK, Meetei R, Carette JE, Porteus MH, Pekrun K, Kay MA. 2021.
514 Improved Genome Editing through Inhibition of FANCM and Members of the BTR
515 Dissolvase Complex. Mol Ther 29:1016–1027.

516 24. Zentilin L, Marcello A, Giacca M. 2001. Involvement of cellular double-stranded DNA break
517 binding proteins in processing of the recombinant adeno-associated virus genome. J Virol
518 75:12279–12287.

519 25. Schwartz RA, Palacios JA, Cassell GD, Adam S, Giacca M, Weitzman MD. 2007. The
520 Mre11/Rad50/Nbs1 complex limits adeno-associated virus transduction and replication. J
521 Virol 81:12936–12945.

522 26. Lentz TB, Samulski RJ. 2015. Insight into the mechanism of inhibition of adeno-associated
523 virus by the Mre11/Rad50/Nbs1 complex. J Virol 89:181–194.

524 27. Karttunen H, Savas JN, McKinney C, Chen Y-H, Yates JR, Hukkanen V, Huang TT, Mohr I.
525 2014. Co-opting the Fanconi anemia genomic stability pathway enables herpesvirus DNA
526 synthesis and productive growth. Mol Cell 55:111–122.

527 28. Cherubini G, Naim V, Caruso P, Burla R, Bogliolo M, Cundari E, Benihoud K, Saggio I,
528 Rosselli F. 2011. The FANC pathway is activated by adenovirus infection and promotes viral
529 replication-dependent recombination. Nucleic Acids Res 39:5459–5473.

530 29. Spriggs CC, Laimins LA. 2017. FANCD2 Binds Human Papillomavirus Genomes and
531 Associates with a Distinct Set of DNA Repair Proteins to Regulate Viral Replication. mBio
532 8:e02340-16.

533 30. Fu S, Phan AT, Mao D, Wang X, Gao G, Goff SP, Zhu Y. 2022. HIV-1 exploits the Fanconi
534 anemia pathway for viral DNA integration. Cell Rep 39:110840.

535 31. Robbez-Masson L, Tie CHC, Conde L, Tunbak H, Husovsky C, Tchasovnikarova IA, Timms RT,
536 Herrero J, Lehner PJ, Rowe HM. 2018. The HUSH complex cooperates with TRIM28 to
537 repress young retrotransposons and new genes. Genome Res 28:836–845.

538 32. Wang GZ, Goff SP. 2016. Transcriptional Silencing of Moloney Murine Leukemia Virus in
539 Human Embryonic Carcinoma Cells. J Virol 91:e02075-16.

540 33. Smith-Moore S, Neil SJD, Fraefel C, Linden RM, Bollen M, Rowe HM, Henckaerts E. 2018.
541 Adeno-associated virus Rep proteins antagonize phosphatase PP1 to counteract KAP1
542 repression of the latent viral genome. Proceedings of the National Academy of Sciences
543 115:E3529–E3538.

544 34. Seczynska M, Bloor S, Cuesta SM, Lehner PJ. 2022. Genome surveillance by HUSH-
545 mediated silencing of intronless mobile elements. 7893. Nature 601:440–445.

546 35. Das A, Vijayan M, Walton EM, Stafford VG, Fiflis DN, Asokan A. 2021. Epigenetic silencing
547 of recombinant AAV genomes by NP220 and the HUSH complex. J Virol JVI0203921.

548 36. Li D-Q, Nair SS, Kumar R. 2013. The MORC family. Epigenetics 8:685–693.

549 37. Xue Y, Gibbons R, Yan Z, Yang D, McDowell TL, Sechi S, Qin J, Zhou S, Higgs D, Wang W.
550 2003. The ATRX syndrome protein forms a chromatin-remodeling complex with Daxx and
551 localizes in promyelocytic leukemia nuclear bodies. Proc Natl Acad Sci U S A 100:10635–
552 10640.

553 38. Hoelper D, Huang H, Jain AY, Patel DJ, Lewis PW. 2017. Structural and mechanistic insights
554 into ATRX-dependent and -independent functions of the histone chaperone DAXX. Nat
555 Commun 8:1193.

556 39. Volk A, Crispino JD. 2015. The role of the chromatin assembly complex (CAF-1) and its p60
557 subunit (CHAF1b) in homeostasis and disease. Biochim Biophys Acta 1849:979–986.

558 40. Geis FK, Sabo Y, Chen X, Li Y, Lu C, Goff SP. 2022. CHAF1A/B mediate silencing of
559 unintegrated HIV-1 DNAs early in infection. Proceedings of the National Academy of
560 Sciences 119:e2116735119.

561 41. Uhlmann F. 2016. SMC complexes: from DNA to chromosomes. Nat Rev Mol Cell Biol
562 17:399–412.

563 42. Yiu SPT, Guo R, Zerbe C, Weekes MP, Gewurz BE. 2022. Epstein-Barr virus BNRF1
564 destabilizes SMC5/6 cohesin complexes to evade its restriction of replication
565 compartments. Cell Reports 38.

566 43. Bentley P, Tan MJA, McBride AA, White EA, Howley PM. 2018. The SMC5/6 Complex
567 Interacts with the Papillomavirus E2 Protein and Influences Maintenance of Viral Episomal
568 DNA. J Virol 92:e00356-18.

569 44. Räschle M, Smeenk G, Hansen RK, Temu T, Oka Y, Hein MY, Nagaraj N, Long DT, Walter JC,
570 Hofmann K, Storchova Z, Cox J, Bekker-Jensen S, Mailand N, Mann M. 2015. DNA repair.
571 Proteomics reveals dynamic assembly of repair complexes during bypass of DNA cross-
572 links. Science 348:1253671.

573 45. Oravcová M, Nie M, Zilio N, Maeda S, Jami-Alahmadi Y, Lazzerini-Denchi E, Wohlschlegel
574 JA, Ulrich HD, Otomo T, Boddy MN. 2022. The Nse5/6-like SIMC1-SLF2 Complex Localizes
575 SMC5/6 to Viral Replication Centers. bioRxiv https://doi.org/10.1101/2022.05.17.492321.

576 46. Hölscher C, Sonntag F, Henrich K, Chen Q, Beneke J, Matula P, Rohr K, Kaderali L, Beil N,
577 Erfle H, Kleinschmidt JA, Müller M. 2015. The SUMOylation Pathway Restricts Gene
578 Transduction by Adeno-Associated Viruses. PLOS Pathogens 11:e1005281.

579 47. Mano M, Ippodrino R, Zentilin L, Zacchigna S, Giacca M. 2015. Genome-wide RNAi
580 screening identifies host restriction factors critical for in vivo AAV transduction.
581 Proceedings of the National Academy of Sciences 112:11276–11281.

582 48. Sanjana NE, Shalem O, Zhang F. 2014. Improved vectors and genome-wide libraries for
583 CRISPR screening. Nat Methods 11:783–784.

584 49. Horlbeck MA, Gilbert LA, Villalta JE, Adamson B, Pak RA, Chen Y, Fields AP, Park CY, Corn
585 JE, Kampmann M, Weissman JS. 2016. Compact and highly active next-generation libraries
586 for CRISPR-mediated gene repression and activation. Elife 5:e19760.

587 50. Li W, Xu H, Xiao T, Cong L, Love MI, Zhang F, Irizarry RA, Liu JS, Brown M, Liu XS. 2014.
588 MAGeCK enables robust identification of essential genes from genome-scale CRISPR/Cas9
589 knockout screens. Genome Biol 15:554.

590 51. Szklarczyk D, Gable AL, Nastou KC, Lyon D, Kirsch R, Pyysalo S, Doncheva NT, Legeay M,
591 Fang T, Bork P, Jensen LJ, von Mering C. 2021. The STRING database in 2021: customizable

592 protein-protein networks, and functional characterization of user-uploaded
593 gene/measurement sets. Nucleic Acids Res 49:D605–D612.

594 52. Shannon P, Markiel A, Ozier O, Baliga NS, Wang JT, Ramage D, Amin N, Schwikowski B,
595 Ideker T. 2003. Cytoscape: a software environment for integrated models of biomolecular
596 interaction networks. Genome Res 13:2498–2504.

597

598 **MAIN FIGURES LEGENDS**

599 **Figure 1. CRISPR screens reveal cellular factors that restrict rAAV transgene expression.**

600 (A) Schematic of genome-wide CRISPR screens using CRISPR KO in A549 human lung
601 adenocarcinoma cells and CRISPRi in K562 myelogenous leukemia cells. Cells were transduced
602 with rAAV2 expressing a fluorescent reporter gene (GFP or tdTomato) and the top 10-20%
603 fluorescent cells were sorted. After 5-7 days, a second round of transduction and sorting was
604 performed before cells were collected for analysis of sgRNA enrichment by next-generation
605 sequencing.

606 (B) MaGeCK gene enrichment scores of the A549 CRISPR KO screen (y-axis) vs. MaGeCK gene
607 enrichment scores of K562 CRISPRi screen (x-axis). Genes with -log10 (enrichment score) > 3 in
608 both screens are highlighted.

609 (C) STRING network for the top 100 hits from both the A549 and the K562 CRISPR screens.
610 Genes were clustered based on high-confidence interactions (STRING confidence cutoff 0.7)
611 and the major gene network is displayed. CRISPR screen enrichment scores for each gene are
612 shown using a color scale. Line thickness indicates confidence of interaction.

613 (D) Heatmap of gene rankings in A549 and K562 CRISPR screens for selected genes related to
614 DNA damage response and other cellular processes.

615

616 **Figure 2. The Fanconi Anemia pathway represses rAAV transgene expression.**

617 (A) rAAV2-tdTomato infection rate or (B) MFI of human WT, FANCA KO and KO UM-SCC1 cells
618 complemented with FANCA transgene (Tg). Cells were infected with rAAV2 (moi=10,000) for
619 48h and tdTomato expression was analyzed by flow cytometry.

620 (C) rAAV2-tdTomato infection rate or (D) MFI of mouse ear fibroblasts (MEF) derived from WT
621 or FANCA KO 129S4/SvJaeSor mice. Cells were infected with rAAV2 (moi=100,000) for 24h and
622 tdTomato expression was analyzed by flow cytometry.
623 (E) rAAV2-tdTomato infection rate or (F) MFI of FA patient-derived head and neck squamous
624 cell carcinoma cells (974 cells), which harbor a FANCA frameshift mutation, as well as of 974
625 cells that were complemented with FANCA transgene (Tg). Cells were infected with rAAV2
626 (moi=10,000) for 48h and tdTomato expression was analyzed by flow cytometry.
627 (G) Quantification of intracellular rAAV genome copies. Transduced cells (moi=10,000) were
628 harvested after 48h, DNA was extracted and AAV and cellular RPPH1 DNA copy numbers were
629 determined by qPCR. Data is combined from 2 independent experiments with 3 biological
630 replicates each.
631 All FACS data are shown as the mean ± s.d. from biological triplicates. P-values were
632 determined by ANOVA with post-hoc Tukey's test for (A)-(B) and unpaired t-test for (C)-(F), and
633 are defined as follows: ns: non-significant; *: <0.05; **: <0.01; ***: <0.001; ****: <0.0001.
634
635 **Figure 3. Knockout of MORC3 and SETDB1 increases rAAV2 transgene expression.**
636 (A) Percentage or (B) MFI of rAAV2-positive cells over time. WT, MORC3 KO or SETDB1 KO A549
637 cells were infected with tdTomato-expressing rAAV2 (moi=10,000) and cells were measured by
638 flow cytometry at day 1, 3, 6 and 8 post-infection.
639 (C) Percentage or (D) MFI of rAAV2-positive WT, MORC3 KO or cDNA-complemented MORC3
640 KO cells. Cells were infected with tdTomato-expressing rAAV2 (moi=10,000) and cells were
641 measured by flow cytometry 24 hpi.

642 (E) Percentage or (F) MFI of rAAV2-positive WT, SETDB1 KO or cDNA-complemented SETDB1 KO
643 cells. Cells were infected with tdTomato-expressing rAAV2 (moi=10,000) and cells were
644 measured by flow cytometry 24 hpi.
645 (G) Percentage or (H) MFI of rAAV2-positive WT, MORC3 KO or SETDB1 KO cells infected with
646 different multiplicities of infection (moi) and measured by flow cytometry 24 hpi.
647 (I) Quantification of intracellular rAAV genome copies in WT A549, MORC3 KO (clone 1) and
648 SETDB1 KO (clone 1). Transduced cells (moi=10,000) were harvested after 48h, DNA was
649 extracted and AAV and cellular RPPH1 DNA copy numbers were determined by qPCR. Data is
650 combined from 2 independent experiments with 3 biological replicates each.
651 FACS data are shown as the mean ± s.d. from biological triplicates (A-F) or from biological
652 duplicates (G-H). P-values were determined by ANOVA with post-hoc Tukey's test and are
653 defined as follows: ns: non-significant; *: <0.05; **: <0.01; ***: <0.001; ****: <0.0001.
654
655 **Figure 4. MORC3 and SETDB1 restrict transgene expression from different rAAV serotypes as**
656 **well as self-complementary rAAV vectors.**
657 (A) Percentage or (B) MFI of WT, MORC3 KO or SETDB1 KO A549 cells infected with rAAV
658 serotypes 1, 5 or 6 (moi=50,000) and analyzed by flow cytometry at 3 dpi.
659 (C) Percentage or (D) MFI of WT, MORC3 KO or SETDB1 KO A549 cells infected with scAAV
660 serotype 2 (moi=10,000) and analyzed by flow cytometry at 3 dpi.
661 All data are shown as the mean ± s.d. from biological triplicates. P-values were determined by
662 ANOVA with post-hoc Tukey's test for each rAAV and are defined as follows: ns: non-significant;
663 *: <0.05; **: <0.01; ***: <0.001; ****: <0.0001.

664

665 **Figure 5. MORC3 and SETDB1 repress transgene expression from lentiviral, adenoviral and**

666 **plasmid vectors.**

667 (A) Percentage or (B) MFI of WT, MORC3 KO or SETDB1 KO A549 cells transduced with different

668 dilutions of a GFP-expressing lentivirus. Fluorescent cells were measured by flow cytometry 3

669 days post-transduction.

670 (C) Percentage or (D) MFI of WT, MORC3 KO or SETDB1 KO A549 cells infected with different

671 moi of a GFP-expressing adenovirus 5 (AdV5-GFP) vector. Cells were analyzed by flow

672 cytometry at 24 hpi.

673 (E) Percentage or (F) MFI of WT, MORC3 KO or SETDB1 KO A549 cells transfected with a GFP

674 encoding plasmid and analyzed by flow cytometry 24h post-transfection.

675 (G) Percentage or (H) MFI of WT, MORC3 KO or SETDB1 KO A549 cells transfected with in-vitro

676 transcribed RFP mRNA and analyzed by flow cytometry 24h post-transfection.

677 All data are shown as the mean ± s.d. from biological triplicates.

678

679 **Figure 6. Knockdown of MORC3 and SETDB1 in primary human fibroblasts increases rAAV**

680 **transgene expression**

681 (A) Percentage of rAAV2-tdTomato positive BJ fibroblasts that were transfected with a non-

682 target siRNA (NT) or siRNAs against MORC3 and SETDB1 4 days prior to rAAV transduction. Cells

683 were analyzed by flow cytometry 36h post-transduction. Data are shown as the mean ± s.d.

684 from biological triplicates. P-values were determined by ANOVA with post-hoc Tukey's test and

685 are defined as follows: ns: non-significant; *: <0.05; **: <0.01; ***: <0.001; ****: <0.0001.

686 (B) Quantification of MORC3 and SETDB1 mRNA levels 4 days after siRNA transfection. Data are

687 shown as the mean ± s.e.m. from biological triplicates.

688

689

690

Figure 1

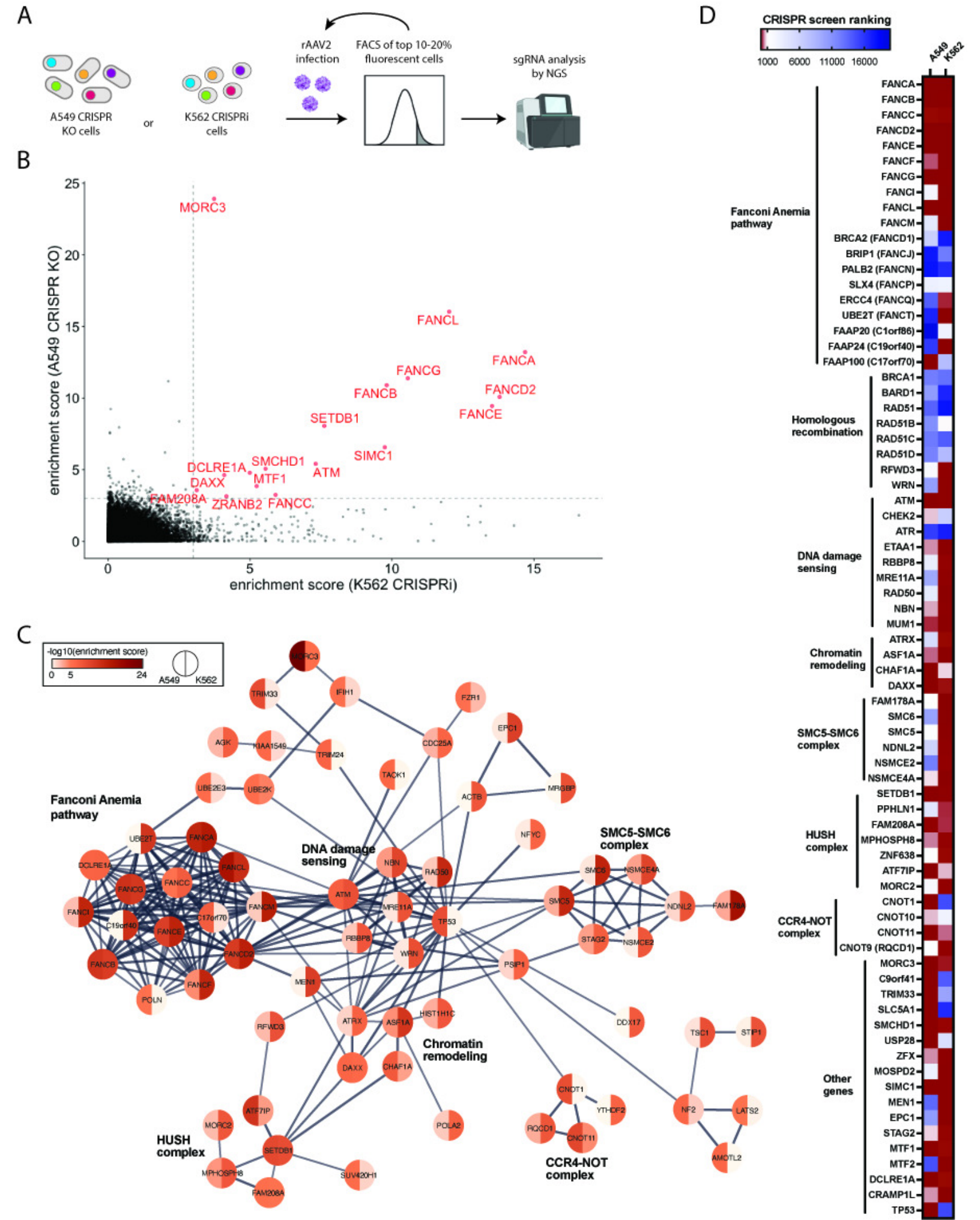
A
A549 CRISPR KO cells
or
K562 CRISPRi cells
rAAV2 infection
FACS of top 10-20% fluorescent cells
sgRNA analysis by NGS
B
enrichment score (A549 CRISPR KO)
enrichment score (K562 CRISPRi)
MORC3
FANCL
FANCA
FANCG
FANCB
FANCD2
FANCE
SETDB1
SIMC1
DCLRE1A
SMCHD1
ATM
DAXX
MTF1
FAM208A
ZRANB2
FANCC
C
-log10(enrichment score)
0 5 24
A549 K562
Fanconi Anemia pathway
DNA damage sensing
SMC5-SMC6 complex
Chromatin remodeling
HUSH complex
CCR4-NOT complex
D
CRISPR screen ranking
1000 6000 11000 16000
A549 K562
Fanconi Anemia pathway
FANCA
FANCB
FANCC
FANCD2
FANCE
FANCF
FANCG
FANCI
FANCL
FANCM
BRCA2 (FANCD1)
BRIP1 (FANCJ)
PALB2 (FANCN)
SLX4 (FANCP)
ERCC4 (FANCQ)
UBE2T (FANCT)
FAAP20 (C1orf86)
FAAP24 (C19orf40)
FAAP100 (C17orf70)
Homologous recombination
BRCA1
BARD1
RAD51
RAD51B
RAD51C
RAD51D
RFWD3
WRN
DNA damage sensing
ATM
CHEK2
ATR
ETAA1
RBBP8
MRE11A
RAD50
NBN
MUM1
Chromatin remodeling
ATRX
ASF1A
CHAF1A
DAXX
SMC5-SMC6 complex
FAM178A
SMC6
SMC5
NDNL2
NSMCE2
NSMCE4A
HUSH complex
SETDB1
PPHLN1
FAM208A
MPHOSPH8
ZNF638
ATF7IP
MORC2
CCR4-NOT complex
CNOT1
CNOT10
CNOT11
CNOT9 (RQCD1)
Other genes
MORC3
C9orf41
TRIM33
SLC5A1
SMCHD1
USP28
ZFX
MOSPD2
SIMC1
MEN1
EPC1
STAG2
MTF1
MTF2
DCLRE1A
CRAMP1L
TP53

Figure 2

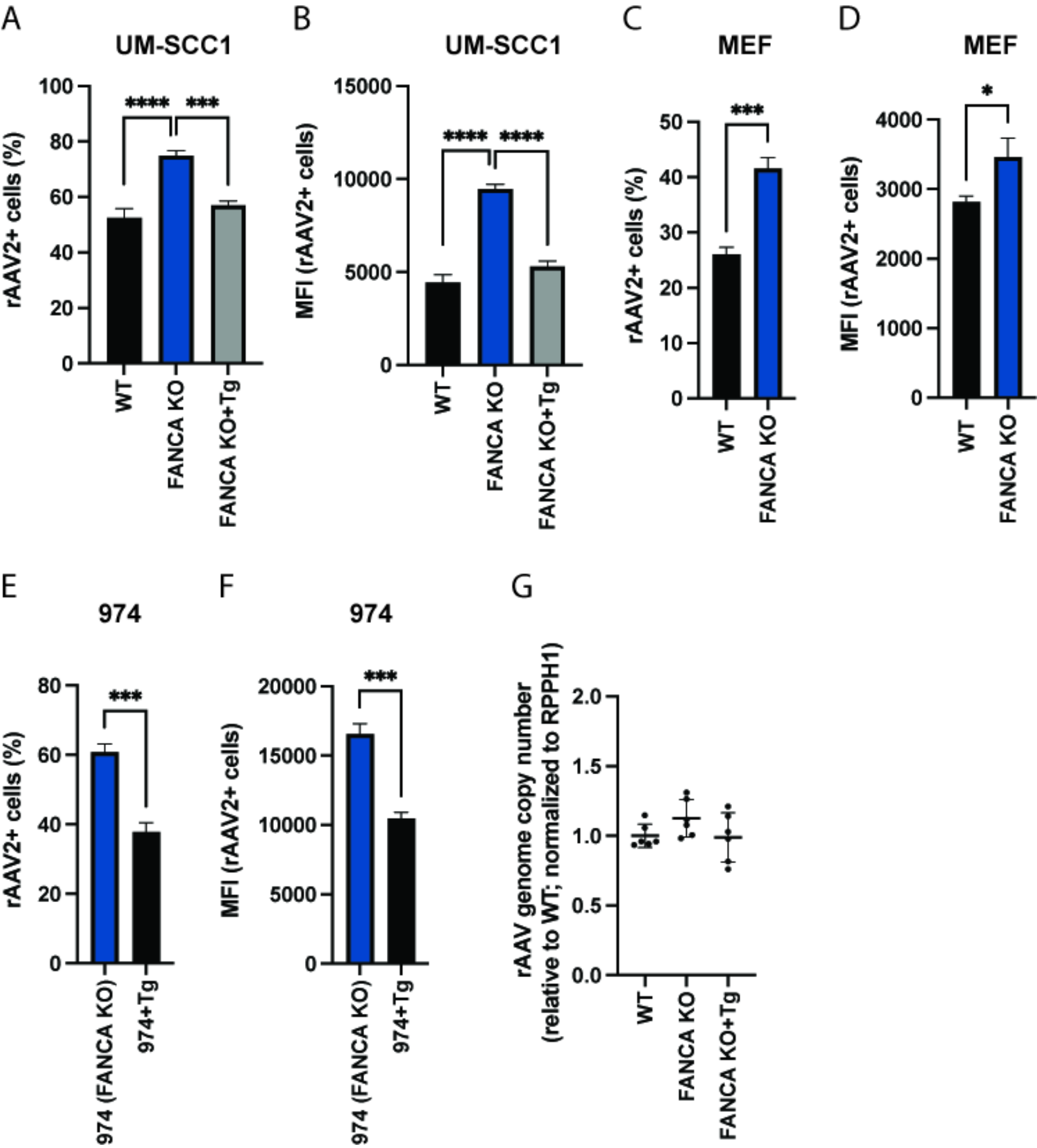
A
UM-SCC1
rAAV2+ cells (%)
100
80
60
40
20
0
****
***
WT
FANCA KO
FANCA KO+Tg
B
UM-SCC1
MFI (rAAV2+ cells)
15000
10000
5000
0
****
****
WT
FANCA KO
FANCA KO+Tg
C
MEF
rAAV2+ cells (%)
50
40
30
20
10
0
***
WT
FANCA KO
D
MEF
MFI (rAAV2+ cells)
4000
3000
2000
1000
0
*
WT
FANCA KO
E
974
rAAV2+ cells (%)
80
60
40
20
0
***
974 (FANCA KO)
974+Tg
F
974
MFI (rAAV2+ cells)
20000
15000
10000
5000
0
***
974 (FANCA KO)
974+Tg
G
rAAV genome copy number
(relative to WT; normalized to RPPH1)
2.0
1.5
1.0
0.5
0.0
WT
FANCA KO
FANCA KO+Tg

Figure 3

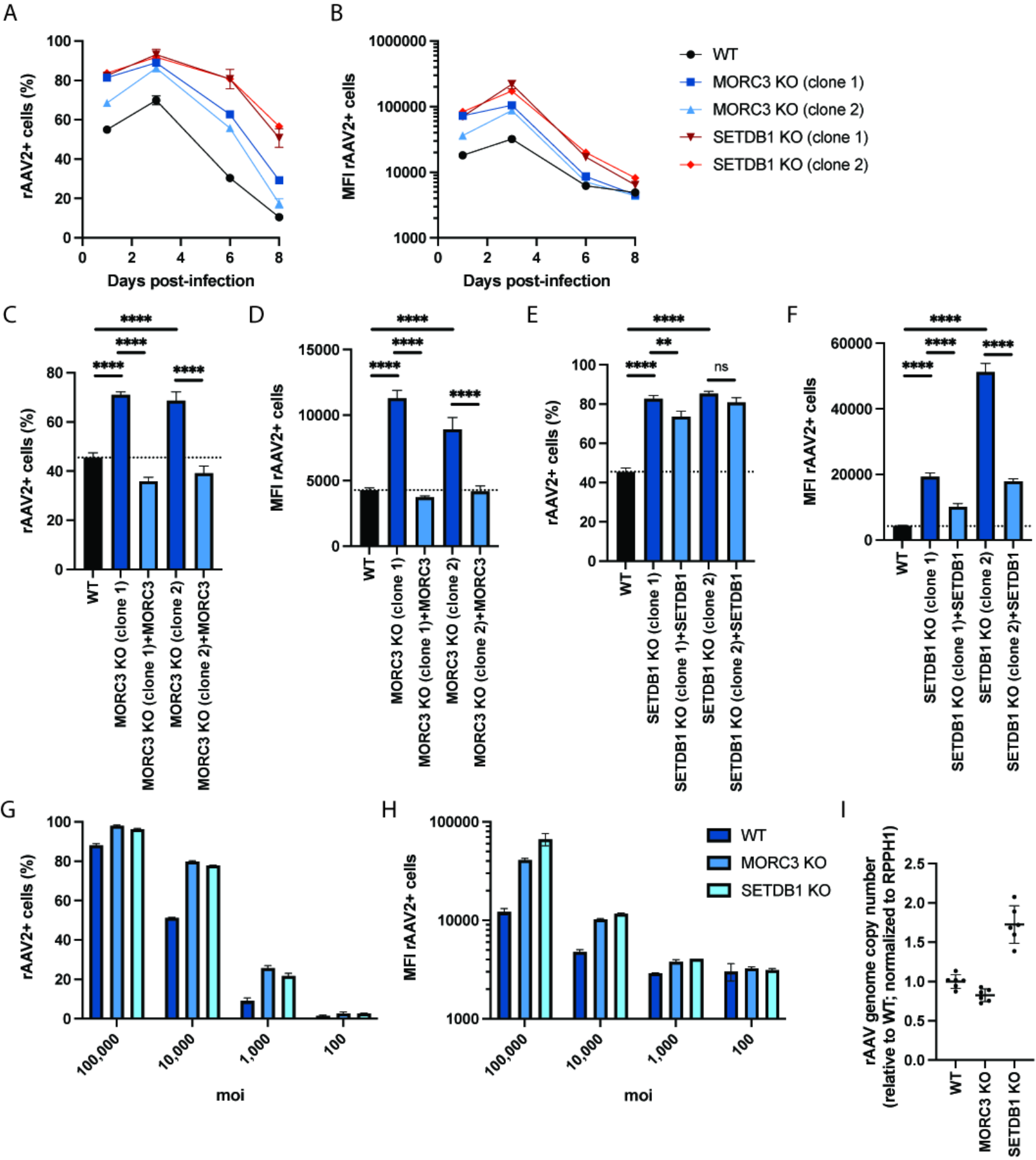
A
rAAV2+ cells (%)
Days post-infection
B
MFI rAAV2+ cells
Days post-infection
WT
MORC3 KO (clone 1)
MORC3 KO (clone 2)
SETDB1 KO (clone 1)
SETDB1 KO (clone 2)
C
rAAV2+ cells (%)
WT
MORC3 KO (clone 1)
MORC3 KO (clone 1)+MORC3
MORC3 KO (clone 2)
MORC3 KO (clone 2)+MORC3
D
MFI rAAV2+ cells
E
rAAV2+ cells (%)
ns
SETDB1 KO (clone 1)
SETDB1 KO (clone 1)+SETDB1
SETDB1 KO (clone 2)
SETDB1 KO (clone 2)+SETDB1
F
MFI rAAV2+ cells
G
rAAV2+ cells (%)
moi
H
MFI rAAV2+ cells
moi
MORC3 KO
SETDB1 KO
I
rAAV genome copy number
(relative to WT; normalized to RPPH1)

Figure 4

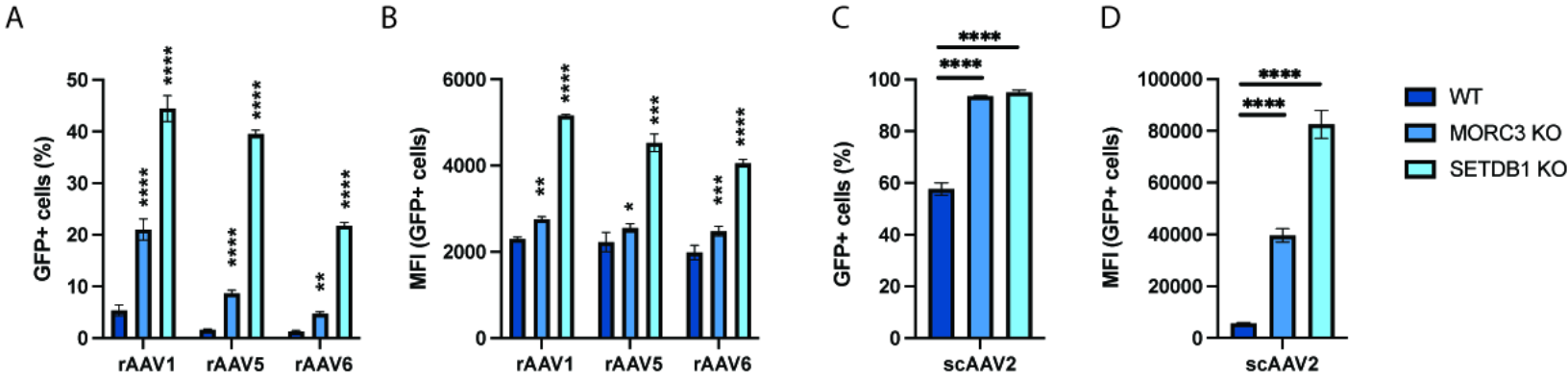
A
GFP+ cells (%)
50
40
30
20
10
0
****
****
****
****
**
****
rAAV1
rAAV5
rAAV6
B
MFI (GFP+ cells)
6000
4000
2000
0
**
****
*
***
***
****
rAAV1
rAAV5
rAAV6
C
GFP+ cells (%)
100
80
60
40
20
0
****
****
scAAV2
D
MFI (GFP+ cells)
100000
80000
60000
40000
20000
0
****
****
scAAV2
WT
MORC3 KO
SETDB1 KO

Figure 5

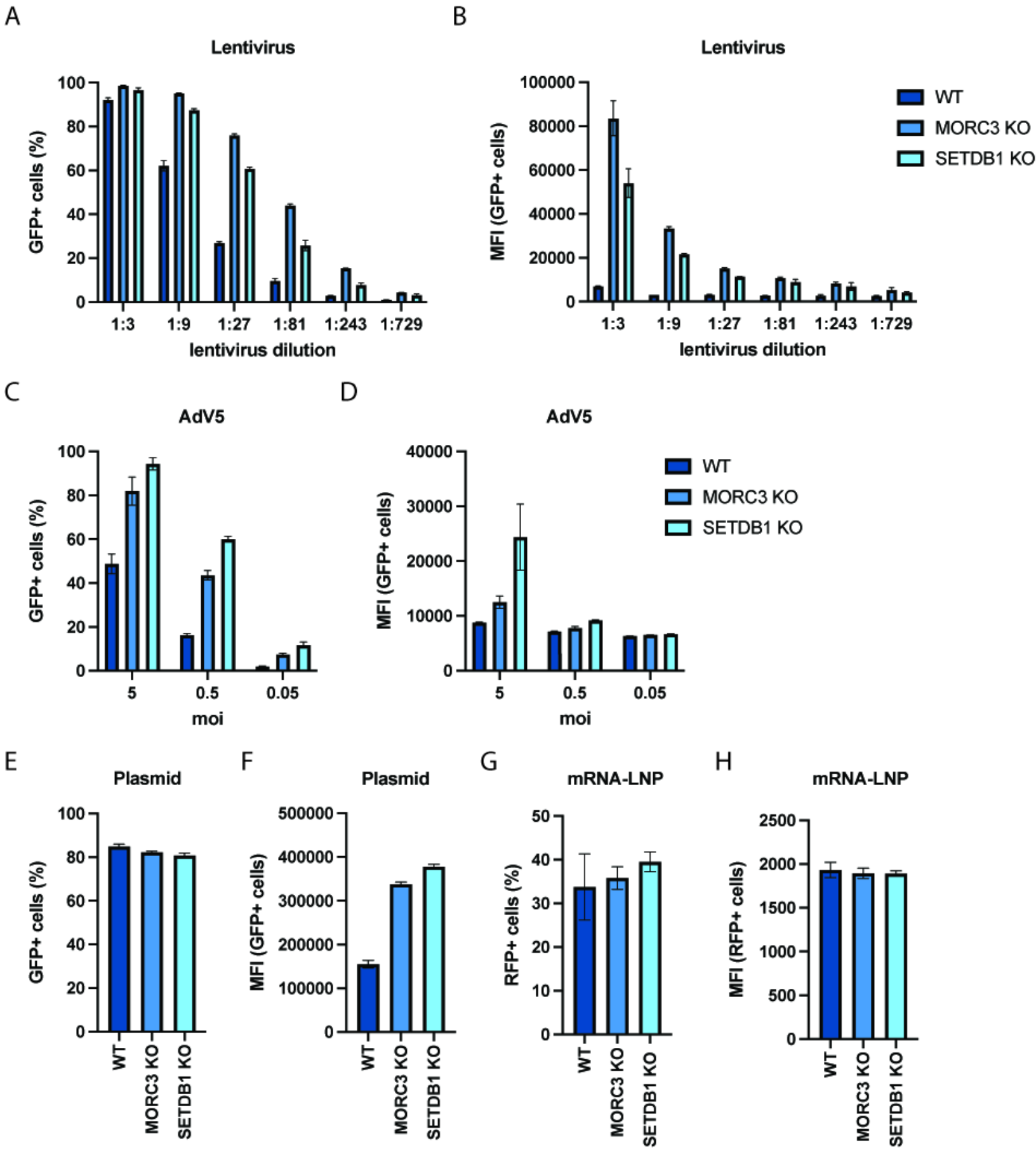
A
Lentivirus
GFP+ cells (%)
100
80
60
40
20
0
1:3
1:9
1:27
1:81
1:243
1:729
lentivirus dilution
B
Lentivirus
MFI (GFP+ cells)
100000
80000
60000
40000
20000
0
1:3
1:9
1:27
1:81
1:243
1:729
lentivirus dilution
WT
MORC3 KO
SETDB1 KO
C
AdV5
GFP+ cells (%)
100
80
60
40
20
0
5
0.5
0.05
moi
D
AdV5
MFI (GFP+ cells)
40000
30000
20000
10000
0
5
0.5
0.05
moi
WT
MORC3 KO
SETDB1 KO
E
Plasmid
GFP+ cells (%)
100
80
60
40
20
0
WT
MORC3 KO
SETDB1 KO
F
Plasmid
MFI (GFP+ cells)
500000
400000
300000
200000
100000
0
WT
MORC3 KO
SETDB1 KO
G
mRNA-LNP
RFP+ cells (%)
50
40
30
20
10
0
WT
MORC3 KO
SETDB1 KO
H
mRNA-LNP
MFI (RFP+ cells)
2500
2000
1500
1000
500
0
WT
MORC3 KO
SETDB1 KO

Figure 6

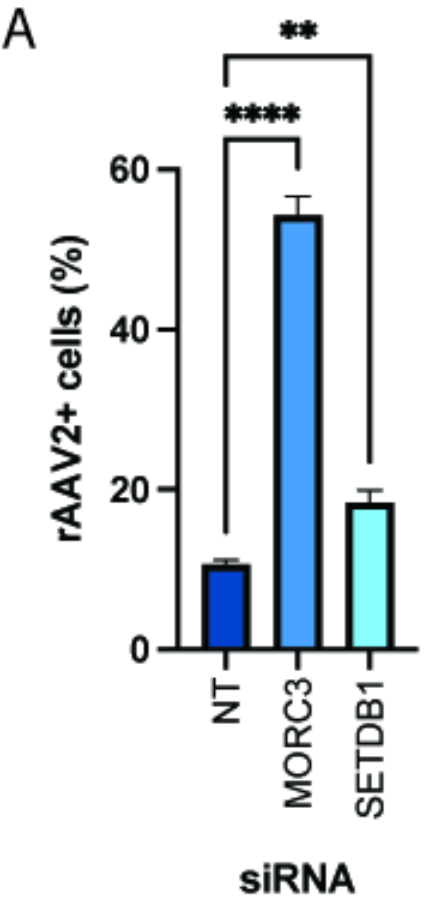
A
**
****
60
40
20
0
rAAV2+ cells (%)
NT
MORC3
SETDB1
siRNA

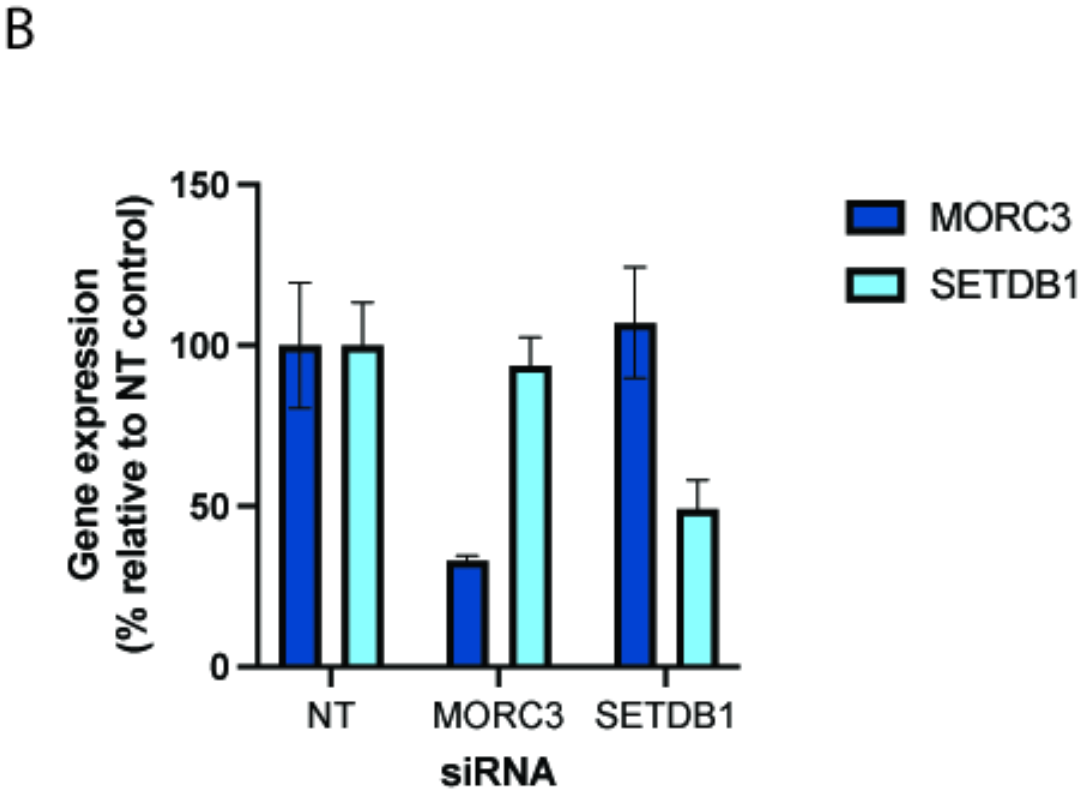
B
150
100
50
0
Gene expression
(% relative to NT control)
NT
MORC3
SETDB1
siRNA
MORC3
SETDB1